

ORIGINAL CONTRIBUTION

Invariant Recognition of Cluttered Scenes by a Self-Organizing ART Architecture: CORT-X Boundary Segmentation

GAIL A. CARPENTER*, STEPHEN GROSSBERG†, AND COUROSH MEHANIAN

Boston University

(Received 11 October 1988; revised and accepted 9 December 1988)

Abstract—A neural network architecture is outlined that self-organizes invariant pattern recognition codes of noisy images. The processing stages are figure-ground separation, boundary segmentation, invariant filtering, and self-organization of a pattern recognition code by an ART 2 network. The article describes a new circuit for boundary segmentation, called the CORT-X filter, that detects, regularizes, and completes sharp (even one-pixel wide) image boundaries in up to 50% noise, while simultaneously suppressing the noise. The CORT-X filter achieves this competence by using nonlinear interactions between multiple spatial scales to resolve a design trade-off that exists between the properties of boundary localization, boundary completion, and noise suppression. The processing levels of the CORT-X filter are analogous to those of the Grossberg-Mingolla Boundary Contour System, but contain only feedforward operations that are easier to implement in hardware. The network nodes in these levels are analogous to cortical simple cells, complex cells, hypercomplex cells, and unoriented and oriented cooperative cells.

Keywords—Neural networks, Pattern recognition, Self-organization, Boundary segmentation, Visual cortex, Boundary contour system, Competition cooperation.

1. INTRODUCTION

This article is the first in a series that develops a self-organizing neural network architecture for invariant pattern recognition in a cluttered environment. Carpenter and Grossberg (1987a) described this architecture (Figure 1a). They reported computer simulation experiments in which an earlier version of the architecture learned to categorize individual image

figures in up to 10% noise that were translated, rotated, or contracted.

Such an architecture sequentially carries out four functionally distinct types of operations:

Step 1. Detach figure from ground.

Step 2. Detect, regularize, and complete figure boundary. Suppress interior and exterior image noise.

Step 3. Filter to give invariance under translation, rotation, and contraction; for example, use a log-polar-Fourier filter (Casasent & Psaltis, 1976; Casavanagh, 1978, 1984; Szu, 1986).

Step 4. Let invariant spectra of the boundary-enhanced, noise-suppressed, detached figures be the input patterns to an ART 2 architecture for stable self-organization of recognition categories (Carpenter & Grossberg, 1987b, 1988). The ART 2 architecture can autonomously learn recognition codes in response to arbitrary orderings of arbitrarily chosen analog or binary input patterns until its full memory capacity is utilized. A vigilance parameter is adjusted to determine how coarse the learned categories will be. Thus the vigilance parameter controls how much deformation in the shape of the figure is tolerated, after deformations due to translation, rotation, or

Requests for reprints should be sent to Gail A. Carpenter, Center for Adaptive Systems, Boston University, 111 Cummington Street, Boston, MA 02215.

*Supported in part by the Air Force Office of Scientific Research (AFOSR F49620-86-C-0037 and AFOSR F49620-87-C-0018), the Army Research Office (ARO DAAL03-88-K-0088), and the National Science Foundation (NSF DMS-86-11959).

†Supported in part by the Air Force Office of Scientific Research (AFOSR F49620-86-C0037 and AFOSR F49620-87-C-0018), the Army Research Office (ARO DAAL03-88-K-0088), and the National Science Foundation (NSF IRI-87-16960).

Acknowledgements: The authors wish to thank Cynthia Suchta and Carol Yanakakis for their valuable assistance in the preparation of the manuscript. We are also grateful to Al Gschwendtner and Wilfrid Veldkamp of M.I.T. Lincoln Laboratory and Mark Coy of the U.S. Army LABC0M-ETDL NSTT for providing computational support.

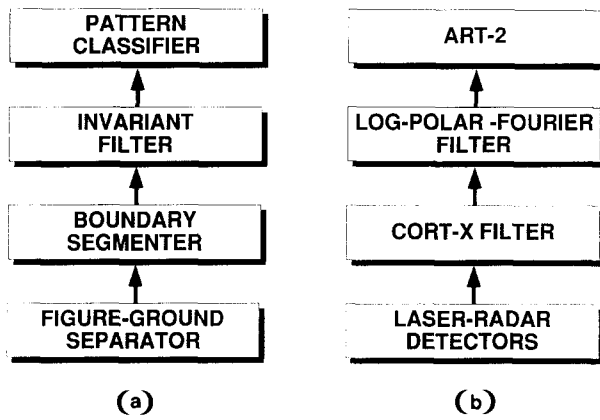


FIGURE 1. System architecture: (a) functional stages; (b) computational realization.

contraction are compensated by the invariant filter. The architecture's recognition learning abilities may be augmented by incorporating additional processing stages capable of reinforcement learning and recall learning (Carpenter & Grossberg, 1988; Grossberg, 1987, 1988).

2. AUTOMATIC SEPARATION OF FIGURE FROM GROUND

The Carpenter and Grossberg (1987a) architecture was used to recognize isolated figures on a noisy, but otherwise uncluttered, background. To use such an architecture, the image figure to be recognized must be detached from the image background. Such figure-ground separation can be automatically achieved, for example, by using laser radar sensors. In particular, let a range detector be focused at the distance of the figure to extract the figure and a contiguous piece of the ground. The figure is then detached from contiguous ground by spatially intersecting the range pattern with a pattern from another detector. A doppler image can be intersected with the range image when the figure is moving. The intensity of laser return can be intersected with the range image when the figure is stationary (Gschwendtner, Harney, & Hull, 1983; Harney, 1980, 1981; Harney & Hull, 1980; Hull & Marcus, 1980; Kolodzy, 1987; Sullivan, D. R., 1980; Sullivan, L. J., 1980, 1981; Sullivan, Harney, & Martin, 1979).

In the present article, we assume that the figure has been separated from the ground by some technique, such as the laser scheme described above. The article describes details of an improved preprocessor stage previously outlined by Carpenter, Grossberg, and Mehanian (1988). The preprocessor stage carries out boundary segmentation, the second step of the architecture (Figure 1b).

3. CORT-X FILTER

We describe a new image preprocessor that detects, regularizes, and completes sharp (even one pixel

wide) image boundaries in up to 50% noise, while simultaneously suppressing the noise. This preprocessor is a modified version of the Boundary Contour System (BCS) of Grossberg and Mingolla (1985). In the Grossberg-Mingolla BCS, nonlinear feedback loops are used to generate sharp and coherent boundaries, so that boundaries may be completed over regions containing no image contrast; for example, where an image figure is partially occluded by another object. The present filter uses only feed-forward operations that are much simpler to fabricate in a real-time analog chip. The filter has a more limited capacity for boundary completion, but one that is adequate for many practical applications. In addition, the present filter employs novel multiple scale interactions to achieve its competence.

This filter is called a CORT-X Filter, both because it is motivated by a neurobiological analysis of visual cortex, and because it uses the operations of Contrast-Oriented-Ratio-Threshold-maximum in an appropriate combination.

4. ORIENTED CONTRAST DETECTOR: SIMPLE CELLS

The network operations in the CORT-X Filter parallel those in the Grossberg-Mingolla BCS. The model's first stage is an oriented contrast detector that is sensitive to the orientation, amount, direction, and spatial scale of image contrast at a given image location. This type of detector may be compared to simple cells in the primate visual cortex. It is modeled herein in the simplest possible way (Figure 2a).

The output of a model simple cell is defined by

$$\max[L_s(x, k) - \alpha_s R_s(x, k) - \beta_s, 0], \quad (1)$$

where x is the position of the receptive field center; k is the receptive field orientation, here chosen to be $0^\circ, 45^\circ, 90^\circ, 135^\circ$; s indexes the size of the receptive fields, here chosen in two sizes; α_s is a contrast parameter such that $1 < \alpha_s$; β_s is a threshold parameter such that $0 < \beta_s < 1$; $L_s(x, k)$ is the total activation of the left half of the receptive field; and $R_s(x, k)$ is the total activation of the right half of the receptive field. In order to write the network in dimensionless form, we define

$$L_s(x, k) = \frac{\int_{\text{left half}} I(y) dy}{\int_{\text{left half}} dy} \quad (2)$$

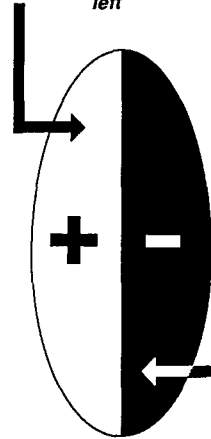
and

$$R_s(x, k) = \frac{\int_{\text{right half}} I(y) dy}{\int_{\text{right half}} dy}, \quad (3)$$

(a) SIMPLE CELL: Sensitive to direction of contrast.

$$\text{output} = \max [L_s(x, k) - \alpha_s R_s(x, k) - \beta_s, 0]$$

$$L_s(x, k) = \frac{\int_{\text{left}} I(y) dy}{\int_{\text{left}} dy}$$



x = position of receptive field center
 k = orientation of receptive field (\rightarrow \searrow \downarrow \swarrow)
 α_s = contrast parameter ($1 < \alpha_s$)
 β_s = threshold parameter ($0 < \beta_s < 1$)
 $I(y)$ = image luminance at position y ($0 \leq I \leq 1$)
 $\max[\dots, 0]$ rectifies output

$$R_s(x, k) = \frac{\int_{\text{right}} I(y) dy}{\int_{\text{right}} dy}$$

(b) SIMPLE CELL:
 These cells respond to the following contrast differences:

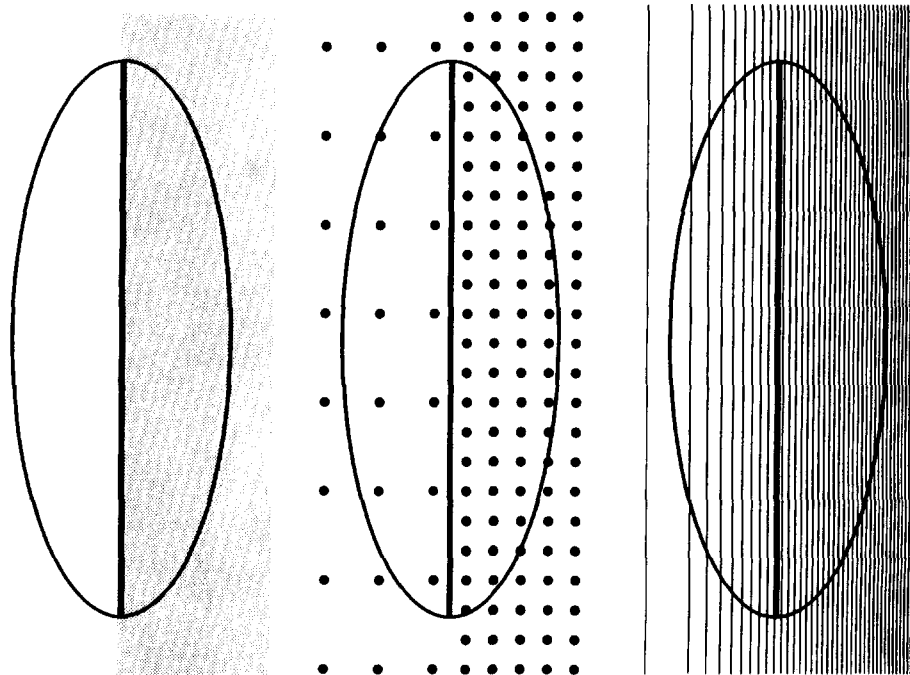


FIGURE 2. Simple cell oriented contrast detector: (a) defining equation; (b) sensitivity to luminance steps, discrete density gradients, and continuous density gradients.

where $I(y)$ is the image luminance at position y , scaled so that $0 \leq I(y) \leq 1$. The function $\max[\dots, 0]$ in (1) rectifies the output signal.

In biological analyses of cortical processing, multiple preprocessing stages intervene between the image luminances impinging upon retinal photorecep-

tors and the cortical simple cells (Hubel & Wiesel, 1977). Alternative detectors with similar properties may also be used, such as a Gabor filter (Daugman, 1980, 1985; Gabor, 1946; Pollen, Andrews, & Feldon, 1978; Pollen & Ronner, 1975, 1981, 1983). For example, in the brightness perception model of

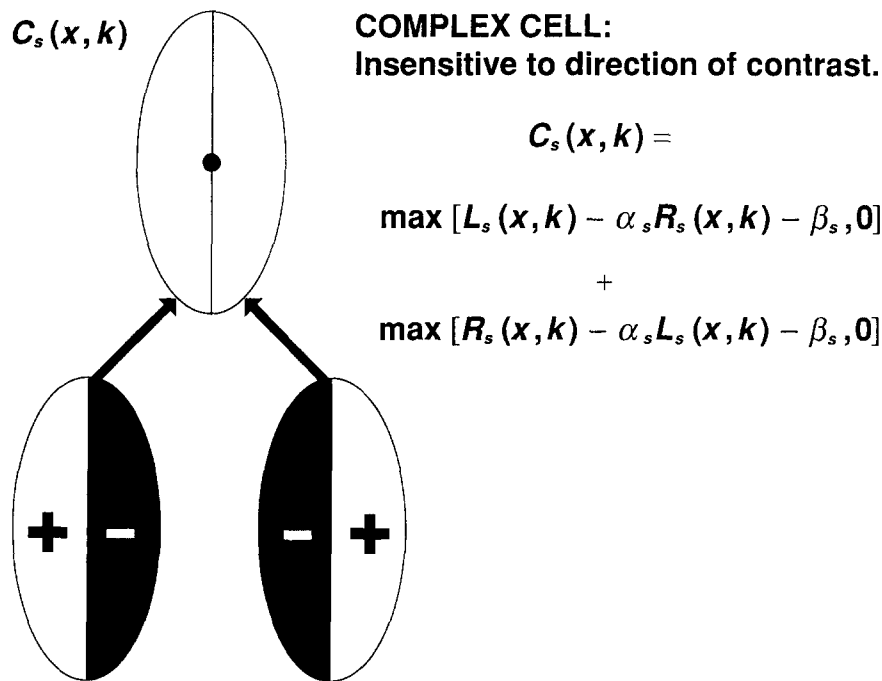


FIGURE 3. Complex cell oriented contrast detector.

Grossberg and Todorović (1988; reprinted in Grossberg, 1988), a shunting on-center off-surround network preprocesses the image to compensate for variable illumination sources before the preprocessed image activates the simple cell level, and the simple cell receptive fields are built up from weighted combinations of oriented difference-of-Gaussian filters.

The simple cell described here responds to luminance steps, dot density differences, gradual changes in luminance, and other contrast changes (Figure 2b) that are oriented almost parallel to the detector's oriented axis.

5. ORIENTED CONTRAST DETECTOR: COMPLEX CELLS

The next processing step consists of a detector that is sensitive to the orientation, amount, and spatial

scale of contrast at a given image location, but not to direction-of-contrast. This type of detector may be compared to complex cells in the primate visual cortex.

To generate a complex cell response $C_s(x, k)$ centered at position x with orientation k and scale s , the activities of a pair of simple cells with the same (x, k) coordinates, but opposite direction-of-contrast (Figure 3) are rectified and added:

$$C_s(x, k) = \max[L_s(x, k) - \alpha_s R_s(x, k) - \beta_s, 0] + \max[R_s(x, k) - \alpha_s L_s(x, k) - \beta_s, 0]. \quad (4)$$

Figure 4 is an image of a truck in 25% noise. Figures 5a and 5b represent the responses of two different sizes of complex cell filters to this image. Figure 6 depicts the size of these two filters relative to an image feature. We now motivate the use of multiple spatial scales in the CORT-X filter.



FIGURE 4. Truck image in 25% noise. The receptive field of each simple cell or complex cell is centered at the upper left-hand corner of a pixel.

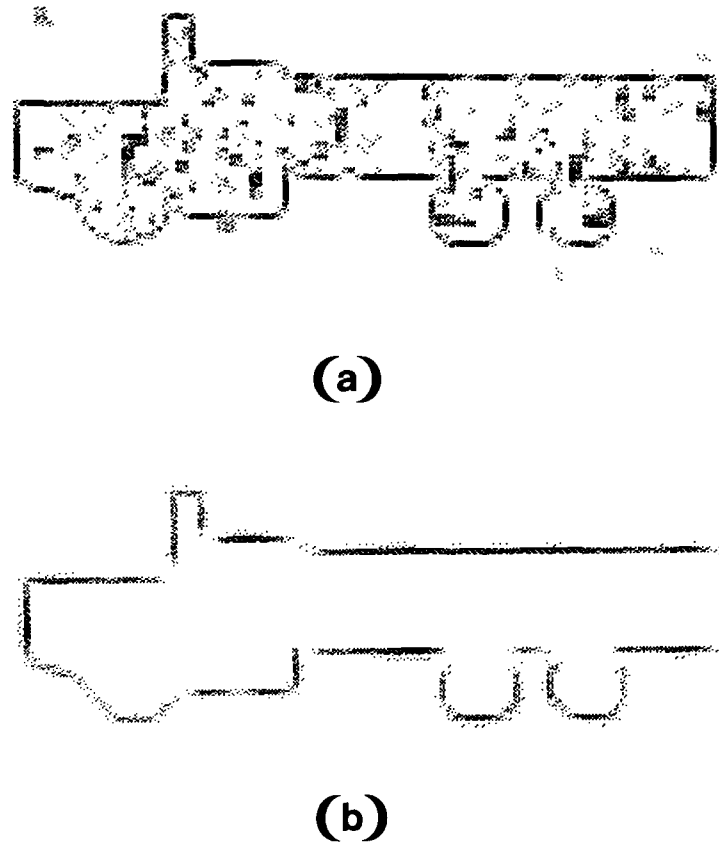


FIGURE 5. Simulated complex cell responses of (a) smaller scale filter; (b) larger scale filter. At each pixel, the grey scale intensity represents the activity of the maximally activated complex cell centered at the pixel's upper left-hand corner. The orientation of this cell is not shown.

6. TRADE-OFF BETWEEN BOUNDARY LOCALIZATION, NOISE SUPPRESSION, AND BOUNDARY COMPLETION

Figure 5 illustrates that the boundaries detected by both filters are incomplete. The smaller filter (Figure 5a) does a better job of boundary localization than

the larger filter (Figure 5b), especially at positions where the boundary has a rapidly changing curvature. On the other hand, the larger filter does a better job of noise suppression and boundary completion.

The better localization by the smaller filter is due to the fact that it estimates boundary location based

MULTIPLE SCALES

TWO DIFFERENT RECEPTIVE FIELD SIZES:
 Accurate boundary segmentation requires multiple spatial scales.

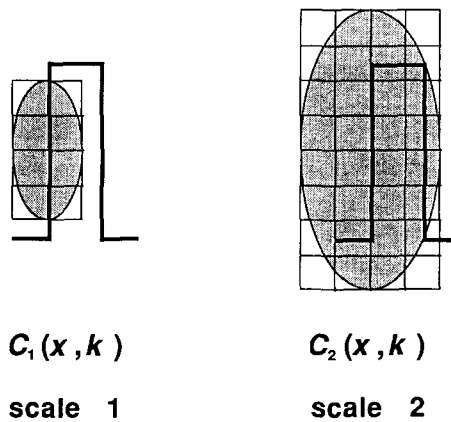


FIGURE 6. Receptive field sizes of two filters relative to pixel size (individual squares) and an illustrative feature.

upon more local contrast estimates than the larger filter. Although all such oriented filters tend to suppress unoriented, or close to unoriented, spatial distributions of noise pixels, the smaller filters may more easily be activated by local fluctuations in the spatial distribution of noise pixels. A larger oriented filter suppresses noise better because it samples the noise distribution more completely. On the other hand, this very property of broader spatial sampling causes poorer boundary localization in regions of high boundary curvature. Thus there exists a trade-off between boundary localization and noise suppression.

In addition, a larger oriented filter can complete a boundary more easily, as a comparison between Figures 5b and 5a illustrates. At the same time, this type of boundary completion can make serious errors in boundary localization in regions of high boundary curvature; for example, consider the wheel boundaries in Figure 5b.

The CORT-X Filter is designed to exploit the good noise suppression and boundary completion properties of a large oriented filter without losing the good positional localization afforded by a small oriented filter.

7. FIRST COMPETITIVE STAGE: HYPERCOMPLEX CELLS FROM SPATIAL COMPETITION

A large oriented filter can suppress noise far from an image boundary. Due to its greater positional uncertainty, however, it cannot efficiently suppress

noise near an image boundary. Thus, neither filter size suppresses noise near a boundary. The relatively high activity of complex cells at an image boundary can be used to suppress the cells near the boundary whose lower activity represents noise (Figure 7). The mechanism whereby this may be accomplished is a variation of the first competitive stage in the Grossberg-Mingolla BCS. The detectors at this first competitive stage may be compared to the hypercomplex cells in the primate visual cortex.

The first competitive stage is realized by an on-center off-surround network (Figure 8a) whereby each complex cell activity $C_s(x, k)$ excites that cell activity $D_s(x, k)$ at the next network level which represents the same position x and orientation k , while inhibiting cell activities $D_s(y, m)$ at nearby positions y that do not lie on the line through position x with orientation k . All orientations m at these positions y are equally inhibited.

The output of the hypercomplex cell at position x , orientation k , and scale s is defined by

$$D_s(x, k) = \frac{C_s(x, k)}{1 + \gamma_s \sum_m \sum_y C_s(y, m) G_s(y, x, k)} \quad (5)$$

The oriented competition kernels $G_s(y, x, k)$, defined in Figure 8b, are 2-dimensional step functions normalized so that

$$\sum_y G_s(y, x, k) = 1. \quad (6)$$

Parameters γ_s specify the strength of the competition. In Figure 8b, symbol x denotes the pixel at

NOISE SUPPRESSION NEAR BOUNDARY

ORIENTED SPATIAL COMPETITION:

Complex cells $C_s(x, k)$ output to an oriented spatial competition which inputs to target cells $D_s(x, k)$. Target cells:

- at a boundary are activated;
- near a boundary are suppressed;
- far from a boundary may be activated by noise.

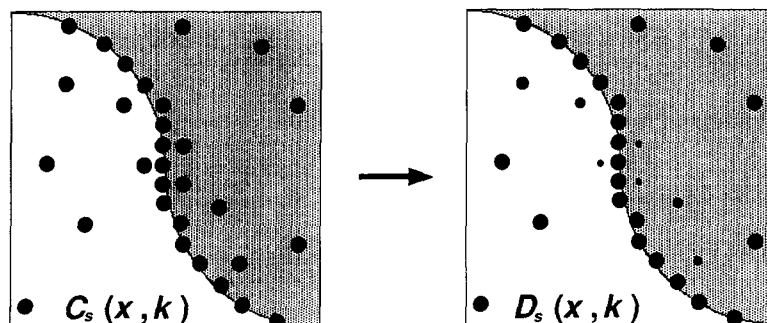
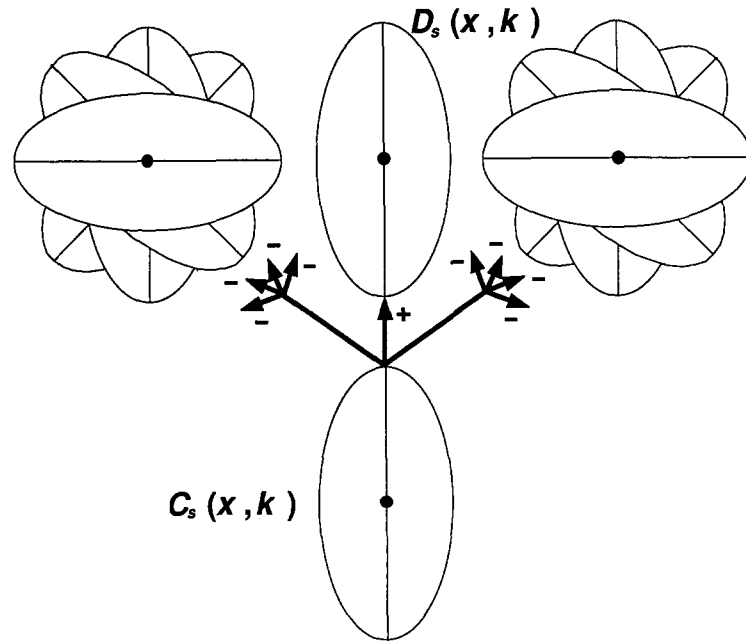


FIGURE 7. Oriented spatial competition inhibits noise pixels near boundary.

(a) **ORIENTED SPATIAL COMPETITION**



(b) **COMPETITION KERNELS**

The competition kernels do not inhibit in the direction along their orientation, i.e., the shaded pixels are inhibited.

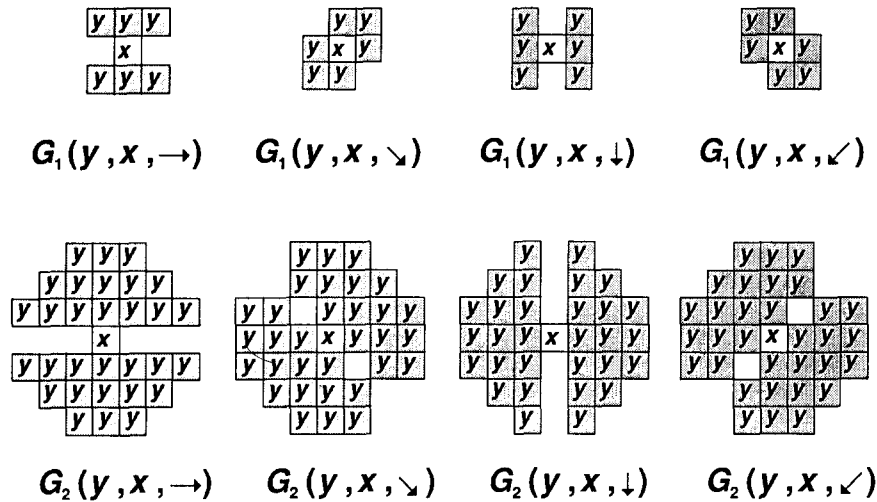


FIGURE 8. First competitive stage: (a) network geometry; (b) interaction kernels.

which the kernel is centered, and y denotes the pixels that are inhibited. The kernel shapes are defined by drawing a circle of diameter 3 or 6 pixels around the kernel center. All pixels which intersect the interior of the circle and which are not on the kernel's axis of orientation are inhibited (and shown as grey).

The off-surround interaction in eq (5) is a shunt-

ing, or divisive, inhibition. The activity $D_s(x, k)$ is the ratio in eq (5) and is restricted to the bounded interval $[0, C_s(x, k)]$.

Figure 9a depicts the hypercomplex activation pattern $D_1(x, k)$ of the smaller filter; Figure 9b depicts the hypercomplex activation pattern $D_2(x, k)$ of the larger filter.

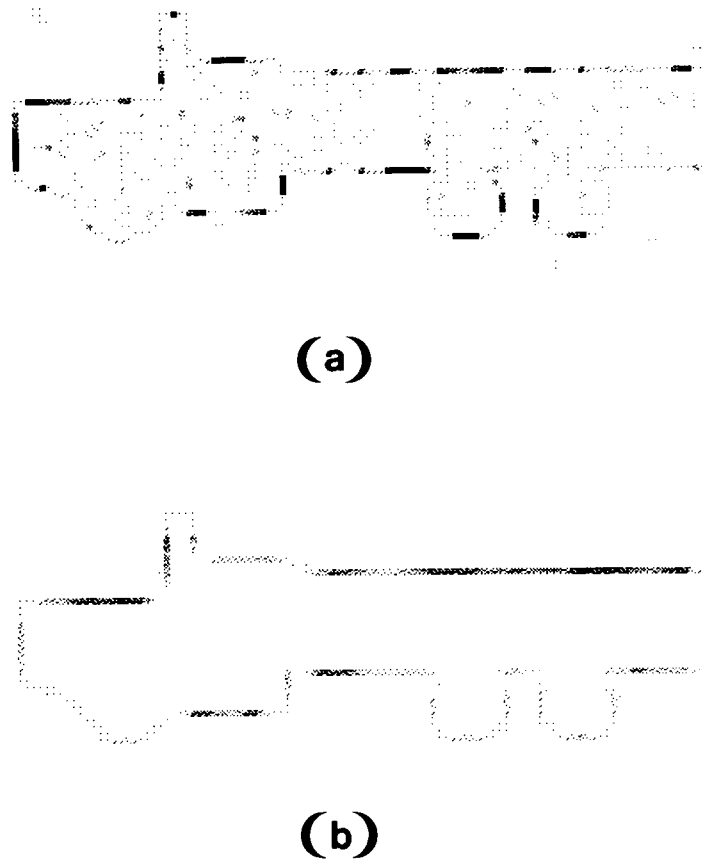


FIGURE 9. Computer simulation of hypercomplex cell response due to oriented spatial competition: (a) smaller filter; (b) larger filter.

8. SELF-SIMILAR COMPETITIVE SCALES

As illustrated in Figure 8b, the size of the on-center off-surround kernels G_1 and G_2 was chosen to scale with the size of the receptive fields C_1 and C_2 , respectively. This property of *self-similarity* generated slightly better results than using a single kernel size G in both scales.

The assumption that self-similar scales occur in biological vision has proven useful in the analysis by Daugman (1985) of image representation by cortical simple cells and by Grossberg and Marshall (1989) of how cortical simple cells and complex cells help to control binocular fusion and rivalry.

9. SECOND COMPETITIVE STAGE: HYPERCOMPLEX CELLS FROM ORIENTATIONAL COMPETITION

The next processing stage is a simplification of the second competitive stage in the Grossberg-Mingolla BCS. It realizes a competition among the oriented activities $D_s(x, k)$ at each position (Figure 10). For simplicity, this process is modeled as a winner-take-all, or choice, process that selects the maximal activity $D_s(x)$ at each position x .

Thus, the hypercomplex cell output from the cell

of position x , orientation k , and scale s at the second competitive stage is

$$D_s(x) = D_2(x, K) = \max_k D_s(x, k), \quad (7)$$

where K denotes the orientation of the maximally activated cell.

10. MULTIPLE SCALE INTERACTION: BOUNDARY LOCALIZATION AND NOISE SUPPRESSION

We now combine the responses of both filter sizes in a way that selects their desirable properties and eliminates their undesirable ones. These properties are summarized in Figure 11. When these filters are used to activate subsequent processing stages, the small scale preserves boundary localization and suppresses noise near the boundary. The large scale suppresses noise away from the boundary and completes colinear boundary segments. This interaction is defined by the equation

$$B_{12}(x) = D_1(x) \sum_y D_2(y) U(y, x). \quad (8)$$

The unoriented excitatory kernel $U(y, x)$, defined

CONTRAST ENHANCEMENT

ORIENTATIONAL COMPETITION:

Competition at each position among the oriented hypercomplex cells selects the most strongly activated orientation.

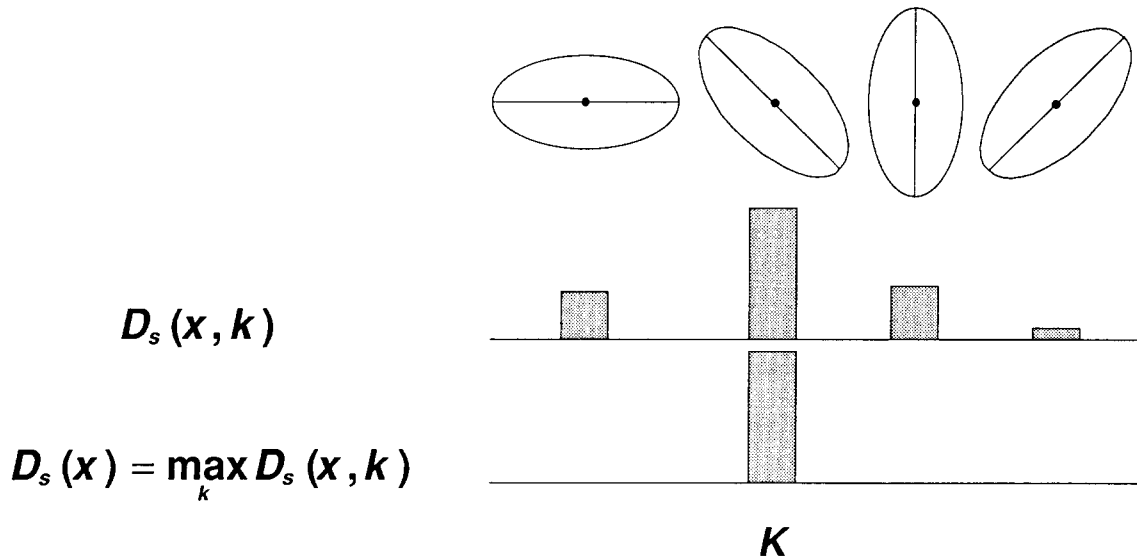


FIGURE 10. Network geometry of second competitive stage.

in Figure 12a, is a 2-dimensional step function normalized so that

$$\sum_y U(y, x) = 1. \tag{9}$$

The factor $D_1(x)$ in eq (8) accurately localizes boundary segments and suppresses noise near the boundary. In other words, $D_1(x)$ is generally positive on the boundary and zero close to the boundary. The

	SMALL SCALE	LARGE SCALE	SMALL + LARGE SCALE
BOUNDARY LOCALIZATION	YES	NOT AT HIGH CURVATURE BOUNDARIES	YES
NOISE SUPPRESSION	NO	YES	YES
BOUNDARY COMPLETION	NOT AT SEGMENTS MISSING DUE TO NOISE	YES	YES

FIGURE 11. Functional properties of individual scales and their combined action.

factor $D_2(y)$ suppresses noise far from the boundary. The product $D_1(x)D_2(y)$ would simultaneously realize both constraints, except for one fact: Due to its poor spatial localization at boundary segments of high curvature, $D_2(x)$ may equal zero at such boundary points x , thereby canceling the good localization properties of $D_1(x)$ at those boundary segments where they are needed most.

This problem is overcome by making the effect of $D_2(y)$ on $D_1(x)$ even *more* spatially diffuse via the kernel $U(y, x)$. This simple device works as follows. The maximal possible spatial error committed by $D_2(y)$ in localizing the boundary grows with the size of $D_2(y)$. Let the size of the kernel $U(y, x)$ scale with the size of $D_2(y)$. Then $\sum_y D_2(y)U(y, x)$ will be positive when $D_1(x)$ is positive, even if $D_2(x)$ equals zero there. Thus, although $\sum_y D_2(y)U(y, x)$ localizes the boundary even less accurately than $D_2(y)$ does, the *product* $D_1(x)\sum_y D_2(y)U(y, x)$ restores this loss of boundary localization. In addition, $U(y, x)$ causes no harm at locations y that are far from the boundary where $D_2(y) = 0$.

Figure 12b depicts the activation pattern of $B_{12}(x)$. The $B_{12}(x)$ pattern provides a significantly less noisy representation of the truck boundary than the $C_1(x)$ pattern in Figure 5a and the $D_1(x)$ pattern in Figure 9a, without a loss of boundary localization.

1ST TERM: BOUNDARY LOCALIZATION PLUS NOISE SUPPRESSION

This term uses the small scale (1) to preserve boundary detail, while using the large scale (2) to suppress noise away from the boundary.

$$B_{12}(x) = D_1(x) \sum_y D_2(y) U(y, x)$$

$$U(y, x) = \text{nearest neighbor kernel, normalized so that } \sum_y U(y, x) = 1$$

y	y	y
y	xy	y
y	y	y

$$U(y, x)$$

(a)

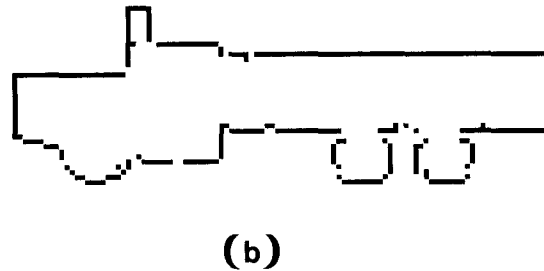


FIGURE 12. Unoriented cooperation $B_{12}(x)$ between both scales: (a) computational properties; (b) computer simulation.

11. ORIENTED LONG-RANGE COOPERATION: BOUNDARY COMPLETION

The boundary representation generated by $B_{12}(x)$ in 25% noise captures the entire boundary except that a few boundary pixels are missing. Such boundary gaps become more and more likely as the noise level is increased. An additional processing stage is introduced to overcome this shortcoming.

This processing stage for boundary completion is a feedforward version of the cooperative-competitive feedback loop (CC Loop) in the Grossberg-Mingolla BCS. In the CC Loop, a long-range oriented cooperation initiates the boundary completion process. The cooperative cells are called *bipole cells*, because they are activated only if enough oriented activation takes place on both sides, or poles, of the cell's receptive field center.

In the absence of feedback interactions, one approach to cooperative boundary completion is to exploit the spatial uncertainty of the larger detectors $D_2(x)$. Because of this spatial uncertainty, these detectors are capable of responding at boundary positions x whose pixels have been deleted by noise. This boundary may, however, be poorly localized. Thus there exists a trade-off between the properties of boundary completion and of boundary localization.

A feedforward operation that overcomes this problem is defined by the equation

$$B_2(x) = D_2(x) \times \max \left[\sum_y D_2(y, K) O(y, x, K) - \delta, 0 \right]. \quad (10)$$

The oriented cooperation kernel $O(y, x, k)$, defined in Figure 13a, is a 2-dimensional step function normalized so that

$$\sum_y O(y, x, k) = 1; \quad (11)$$

δ is a cooperation threshold; and K is the orientation corresponding to the maximal activity $D_2(x, K)$ defined in eq (7).

Function $B_2(x)$ in eq (10) depends only upon responses of the larger detectors $D_2(x)$. Taken individually, these detectors would provide poorly localized responses along boundary segments of high curvature. Due to the oriented cooperation defined in eq (10), however, a detector $D_2(x)$ can activate $B_2(x)$ only if it receives cooperative support from colinear detectors $D_2(y)$ with the same orientational preference. Consequently, the detector $B_2(x)$ is activated only along those accurately localized boundary segments that provide enough cooperative support, as illustrated in Figure 13b.

COOPERATION KERNELS

Sufficient colinear activity of cells $D_2(x, k)$ along a particular orientation will complete gaps in $B_{12}(x)$ along that direction.

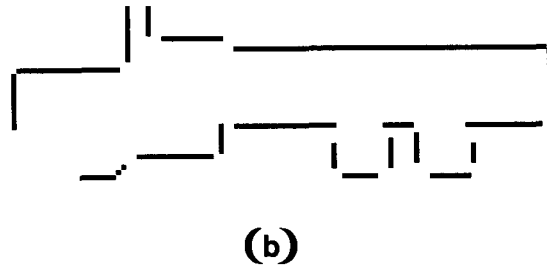
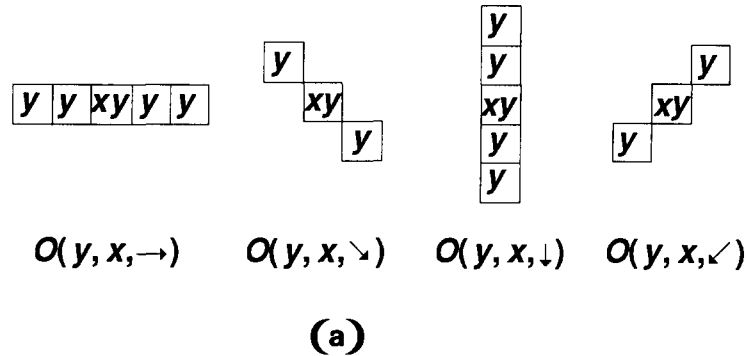


FIGURE 13. Oriented cooperation $B_2(x)$ within larger scale: (a) cooperation kernels; (b) computer simulation.

12. THE CORT-X FILTER

The output of the CORT-X Filter is the rectified sum of $B_{12}(x)$ and $B_2(x)$, namely

$$B(x) = 1[B_{12}(x) + B_2(x)] \quad (12)$$

where $1(w)$ is the Heaviside function

$$1(w) = \begin{cases} 1 & \text{if } w > 0 \\ 0 & \text{if } w = 0 \end{cases} \quad (13)$$

Figure 14 shows how the responses of $B_{12}(x)$ in Figure 12b and $B_2(x)$ in Figure 13b combine to generate the boundary representation, $B(x)$, of the image in Figure 4 that was corrupted by 25% noise.

Figures 15–17 summarize the CORT-X Filter boundary representations of four different trucks in 0%, 20%, and 40% noise that have been translated, rotated, and contracted.

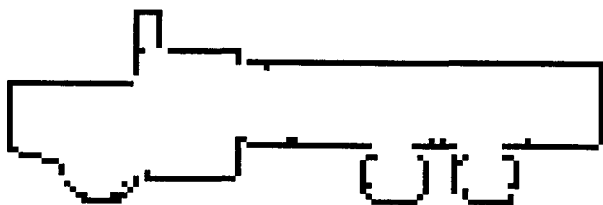


FIGURE 14. Computer simulation of CORT-X filter output $B(x)$.

simulations are listed in Table 1. Boundary reconstruction begins to fail at around 50% noise due to the fact that increasingly large segments of the boundary may be corrupted as the noise level becomes increasingly large. At these very high noise levels the vigilance parameter of the ART 2 archi-

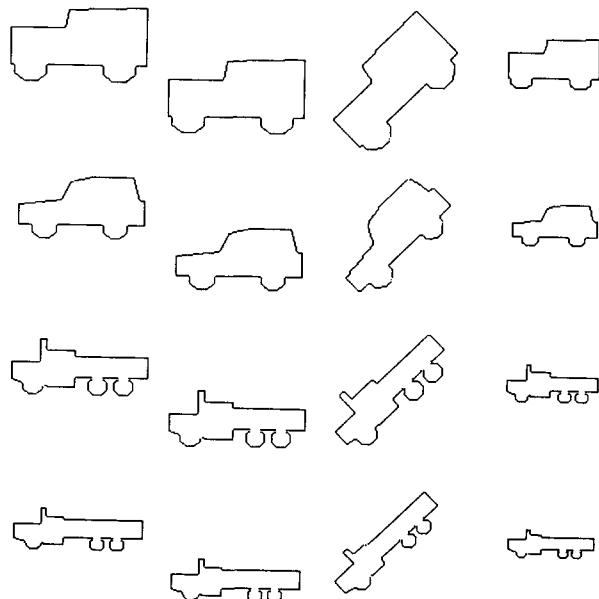


FIGURE 15. Computer simulation of CORT-X filter output of four trucks in 0% noise that have been translated, rotated, and contracted.

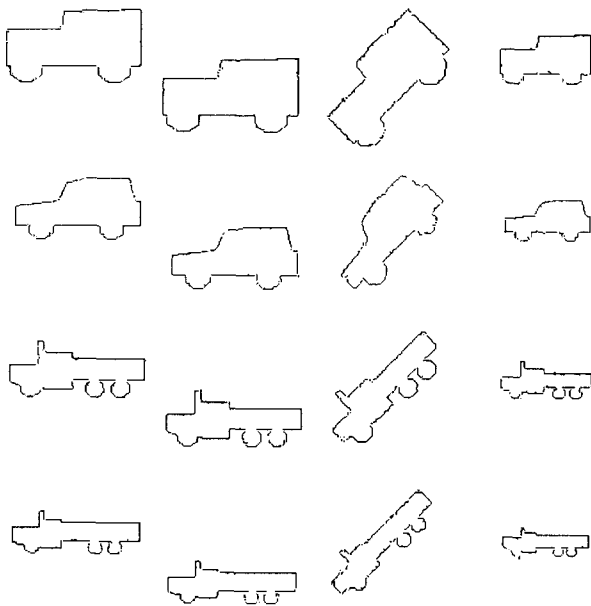


FIGURE 16. Same as Figure 15 in 20% noise.

texture (Carpenter & Grossberg, 1987b) may be set, if desired, to accept a degree of image deformation that includes the expected degree of boundary distortion after CORT-X Filter processing.

13. CONCLUDING REMARKS

Subsequent articles in this series will demonstrate how CORT-X filtered images may be used to self-organize invariant recognition categories using variants of the system architecture that is outlined in

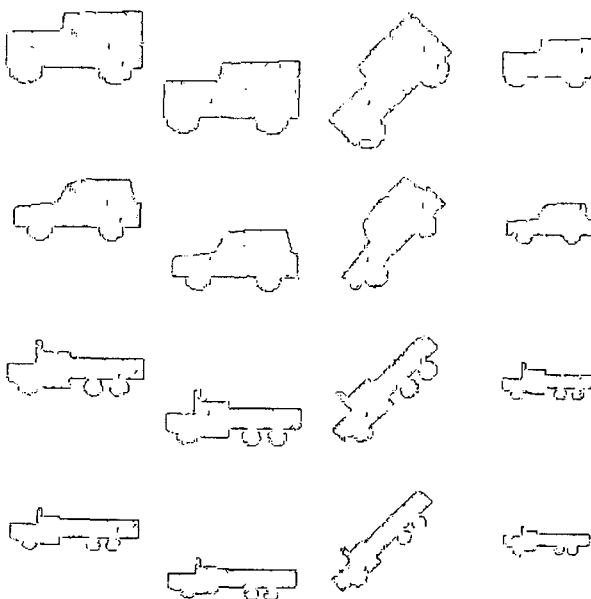


FIGURE 17. Same as Figure 15 in 40% noise.

TABLE 1
Parameters Used in All Simulations

$\alpha_1 = 1.4$
$\alpha_2 = 2.0$
$\beta_1 = \beta_2 = 0.3$
$\gamma_1 = \gamma_2 = 0.3$
$\delta = 0.012$

Figure 1. CORT-X filtering may also be useful as a preprocessor for other adaptive pattern recognition schemes.

The CORT-X filter is also of interest in its own right as a feedforward multiscale version of the Grossberg-Mingolla Boundary Contour System. From this perspective, the CORT-X filter clarifies how boundary contour operations may be used to resolve the fundamental design trade-off that exists between boundary localization, boundary completion, and noise suppression.

REFERENCES

- Carpenter, G. A., & Grossberg, S. (1987a). Invariant pattern recognition and recall by an attentive self-organizing ART architecture in a nonstationary world. In M. Caudill & C. Butler (Eds.), *Proceedings of the IEEE International Conference on Neural Networks, II* (pp. 737-745). New York: IEEE.
- Carpenter, G. A., & Grossberg, S. (1987b). ART 2: Self-organization of stable category recognition codes for analog input patterns. *Applied Optics*, **26**, 4919-4930.
- Carpenter, G. A., & Grossberg, S. (1988). The ART of adaptive pattern recognition by a self-organizing neural network. *Computer*, **21**, 77-88.
- Carpenter, G. A., Grossberg, S., & Mehanian, C. (1988). Self-organization of invariant recognition categories for noisy images by an adaptive resonance theory (ART) architecture. *Neural Networks*, **1** (Suppl. 1), 15.
- Casasent, D., & Psaltis, D. (1976). Position, rotation, and scale invariant optical correlations. *Applied Optics*, **15**, 1793-1799.
- Cavanagh, P. (1978). Size and position invariance in the visual system. *Perception*, **7**, 167-177.
- Cavanagh, P. (1984). Image transforms in the visual system. In P. C. Dodwell & T. Caelli (Eds.), *Figural synthesis* (pp. 185-218). Hillsdale, NJ: Erlbaum.
- Daugman, J. G. (1980). Two-dimensional spectral analysis of cortical receptive field profiles. *Vision Research*, **20**, 847-856.
- Daugman, J. G. (1985). Uncertainty relation for resolution in space, spatial frequency, and orientation optimized by two-dimensional visual cortical filters. *Journal of the Optical Society of America*, **2**, 1160-1169.
- Gabor, D. (1946). Theory of communication. *IEEE Transactions*, **93**, 429-457.
- Grossberg, S. (Ed.). (1987). *The adaptive brain, I: Cognition, learning, reinforcement, and rhythm*. Amsterdam: Elsevier/North-Holland.
- Grossberg, S. (Ed.). (1988). *Neural networks and natural intelligence*. Cambridge, MA: MIT Press.
- Grossberg, S., & Marshall, J. (1989). Stereo boundary fusion by

- cortical complex cells: A system of maps, filters, and feedback networks for multiplexing distributed data. *Neural Networks*, **2**, 29–51.
- Grossberg, S., & Mingolla, E. (1985). Neural dynamics of perceptual grouping: Textures, boundaries, and emergent segmentations. *Perception and Psychophysics*, **38**, 141–171.
- Grossberg, S., & Todorović, D. (1988). Neural dynamics of 1-D and 2-D brightness perception: A unified model of classical and recent phenomena. *Perception and Psychophysics*, **43**, 241–277.
- Gschwendtner, A. B., Harney, R. C., & Hull, R. J. (1983). Coherent IR radar technology. In D. K. Killinger & A. Mooradian (Eds.), *Optical and laser remote sensing*. New York: Springer-Verlag.
- Harney, R. C. (1980). Infrared airborne radar. *Proceedings of the IEEE Electronic and Aerospace Systems Conference* (pp. 462–471).
- Harney, R. C. (1981). Military applications of coherent infrared radar. *Physics and Technology of Coherent Infrared Radar (SPIE Proceedings)*, **300**, 2–11.
- Harney, R. C., & Hull, R. J. (1980). Compact infrared radar technology. *CO₂ Laser Devices and Applications (SPIE Proceedings)*, **227**, 162–170.
- Hubel, D. H., & Wiesel, T. N. (1977). Functional architecture of macaque monkey visual cortex. *Proceedings of the Royal Society of London (B)*, **198**, 1–59.
- Hull, R. J., & Marcus, S. (1980). A tactical 10.6 micrometer imaging radar. *Proceedings of the IEEE National Aerospace and Electronics Conference*, **2**, 662–668.
- Kolodzy, P. (1987). Multidimensional machine vision using neural networks. In M. Caudill & C. Butler (Eds.), *Proceedings of the IEEE International Conference on Neural Networks, II*, (pp. 747–758). New York: IEEE.
- Pollen, D. A., Andrews, B. W., & Feldon, S. E. (1978). Spatial frequency selectivity of periodic complex cells in the visual cortex of the cat. *Vision Research*, **18**, 665–682.
- Pollen, D. A., & Ronner, S. F. (1975). Periodic excitability changes across the receptive fields of complex cells in the striate and parastriate cortex of the cat. *Journal of Physiology (London)*, **245**, 667–697.
- Pollen, D. A., & Ronner, S. F. (1981). Phase relationships between adjacent simple cells in the visual cortex. *Science*, **212**, 1409–1411.
- Pollen, D. A., & Ronner, S. F. (1983). Visual cortical neurons as localized spatial frequency filters. *IEEE Transactions on Systems, Man, and Cybernetics*, **SMC-13**, 907–916.
- Sullivan, D. R. (1980). Active 10.6 micrometer image processing. *Imaging Processing and Missile Guidance (SPIE Proceedings)*, **238**, 103–117.
- Sullivan, L. J. (1980). Infrared coherent radar. *CO₂ Laser Devices and Applications (SPIE Proceedings)*, **227**, 148–161.
- Sullivan, L. J. (1981). Firepond laser radar. *Electro/81 Conference Record*, Session 34.
- Sullivan, D. R., Harney, R. C., & Martin, J. S. (1979). Real-time quasi-3-dimensional display of infrared radar images. *Real-Time Signal Processing, II (SPIE Proceedings)*, **180**, 57–65.
- Szu, H. (1986). Three layers of vector output product neural networks for optical pattern recognition. In H. Szu (Ed.), *Optical and hybrid computing* (pp. 312–330). Bellingham, WA: SPIE.